



# Vibration amplitude and induced temperature limitation of high power air-borne ultrasonic transducers<sup>☆</sup>



Saber Saffar<sup>\*</sup>, Amir Abdullah

Mechanical Engineering Faculty, Amirkabir University of Technology, 424, Hafez Avenue, Tehran, Iran

## ARTICLE INFO

### Article history:

Received 23 October 2012

Received in revised form 2 April 2013

Accepted 9 April 2013

Available online 19 April 2013

### Keywords:

Acoustic impedance

Air borne ultrasonic transducers

Genetic algorithm (GA)

Internal loss

Amplitude of vibration

## ABSTRACT

The acoustic impedances of matching layers, their internal loss and vibration amplitude are the most important and influential parameters in the performance of high power airborne ultrasonic transducers. In this paper, the optimum acoustic impedances of the transducer matching layers were determined by using a genetic algorithm, the powerful tool for optimizing domain. The analytical results showed that the vibration amplitude increases significantly for low acoustic impedance matching layers. This enhancement is maximum and approximately 200 times higher for the last matching layer where it has the same interface with the air than the vibration amplitude of the source, lead zirconate titanate-pizo electric while transferring the 1 kW is desirable. This large amplitude increases both mechanical failure and temperature of the matching layers due to the internal loss of the matching layers. It has analytically shown that the temperature in last matching layer with having the maximum vibration amplitude is high enough to melt or burn the matching layers. To verify suggested approach, the effect of the amplitude of vibration on the induced temperature has been investigated experimentally. The experimental results displayed good agreement with the theoretical predictions.

© 2013 Elsevier B.V. All rights reserved.

## 1. Introduction

Ultrasonic transducers are widely used in numerous applications, including machining, forming, medical and non-destructive testing applications. The utility of this technology may have been widespread if the sound waves could transfer through the air with the appropriate performance. However, certain limitations exist in the choice of intermediate layers for impedance matching between the ultrasonic piezo-ceramic transducers and the medium through which the ultrasonic energy must be transmitted.

Depending on the loading medium, quarter-wave matching layers are usually proposed [1]. However, certain researchers have become interested in matching the impedance of the ultrasonic transducer with gas medium [2–8]. Theoretically, it is possible to use one-, two- or multi-layer transducer construction. Other researchers have focused on the theoretical or experimental design of narrow or broadband airborne ultrasonic transducers using one or two matching layers [9–11]. Additional studies have concentrated on the fabrication of new materials with both low acoustic

impedance and attenuation values [12–15]. Another subset of researchers has attempted to increase the rate of energy transmission through the air and to develop low acoustic impedance materials with a low attenuation coefficient [16].

Moreover, other researchers have shown interest in the application of airborne ultrasonic transducers in industry and have aimed to reduce the existing difficulties in the use of these devices [17–23]. They use thin membranes in the design to solve the problem. However, the modified products are less robust and more easily damaged.

There are in general two types of airborne ultrasonic transducers; low power and high power transducers. Literature shows that massive studies have been done on low power airborne ultrasonic transducers for nondestructive testing applications, while little effort has been conducted to investigate the airborne ultrasonic transducer with high power.

In general, last matching layers are low acoustic impedance materials in airborne ultrasonic transducers. Furthermore, these materials show high attenuation generally, and especially high amplitude of vibration in high power airborne ultrasonic transducers. Therefore, heat generation is one of the significant issues in high power airborne ultrasonic transducers.

The main contribution of this paper is to investigate the heat generation in matching layers determined based on a genetic algorithm (GA) for a high power airborne ultrasonic transducer (1 kW). Therefore, the identification of appropriate matching layers based

<sup>☆</sup> This is an open-access article distributed under the terms of the Creative Commons Attribution-NonCommercial-No Derivative Works License, which permits non-commercial use, distribution, and reproduction in any medium, provided the original author and source are credited.

<sup>\*</sup> Corresponding author.

E-mail address: [saber.saffar@gmail.com](mailto:saber.saffar@gmail.com) (S. Saffar).

on the GA and heat generation is of interest. In addition, effects of the amplitude of vibration and internal loss of matching layers on temperature distribution for different matching layers are investigated. A set of experiments are performed to verify the analytical approach and results of theoretical investigations and experiments are compared.

## 2. Theory

### 2.1. Sound power transmission to the air

In order to determine the appropriate acoustic impedances for matching the actuator source (PZT) to the air, it is necessary to calculate the input mechanical impedance for each set of proposed matching layers. If the input mechanical impedance of the set of matching layers is close to the acoustic impedance of the PZT, then this set of matching layers is desirable, otherwise it should be change to another one. Hence, calculating of the input mechanical impedance of a layer is determined and then it is derived for multi layers. The input mechanical impedance for one degree of freedom system is [24]:

$$\begin{aligned} Z_m &= R_m + jX_m \\ X_m &= (\omega m - k_{spring}/\omega) \end{aligned} \quad (1)$$

Fig. 1 illustrates the damped oscillating system at the end of an excited cylinder layer. If this system is added to the end of the excited simple layer (see Fig. 1), then the mechanical impedance at the interface  $Z_m$  is calculated from Eq. (1). The general solution of displacement and the boundary condition are written as [24]:

$$\begin{aligned} u(x, t) &= Ae^{j(\omega t - k^*x)} + Be^{j(\omega t + k^*x)} \\ k^* &= k_1 + k_2j \\ \begin{cases} F(0, t) = -\rho s c^{*2} \frac{\partial u}{\partial x} \Big|_{x=0} \\ \frac{\partial u}{\partial x} \Big|_{x=L} = \frac{-Z_m}{\rho s c^{*2}} \left( \frac{\partial u}{\partial t} \Big|_{x=L} \right) \end{cases} \end{aligned} \quad (2)$$

where  $A$  and  $B$  are amplitudes of the incident and reflected waves, respectively,  $F$  is the force and  $s$ ,  $\rho$ ,  $k^*$  and  $c^*$  are parameters of the cross section, density, complex wave number and complex speed of sound of layer respectively.

By assuming the boundary condition, the solution is rewritten as:

$$\begin{aligned} u(x, t) &= (A_1 + jA_2)e^{j(\omega t - (k_1 + jk_2)x)} + (B_1 + jB_2)e^{j(\omega t + (k_1 + jk_2)x)} \\ &= (A_1 + jA_2)e^{k_2x}e^{j(\omega t - k_1x)} + (B_1 + jB_2)e^{-k_2x}e^{j(\omega t + k_1x)} \\ &= A_1e^{k_2x}\cos(\omega t - k_1x) - A_2e^{k_2x}\sin(\omega t - k_1x) + B_1e^{-k_2x} \\ &\quad \times \cos(\omega t + k_1x) - B_2e^{-k_2x}\sin(\omega t + k_1x) + j[A_1e^{k_2x} \\ &\quad \times \sin(\omega t - k_1x) + A_2e^{k_2x}\cos(\omega t - k_1x) + B_1e^{-k_2x} \\ &\quad \times \sin(\omega t + k_1x) + B_2e^{-k_2x}\cos(\omega t + k_1x)] \end{aligned} \quad (3)$$

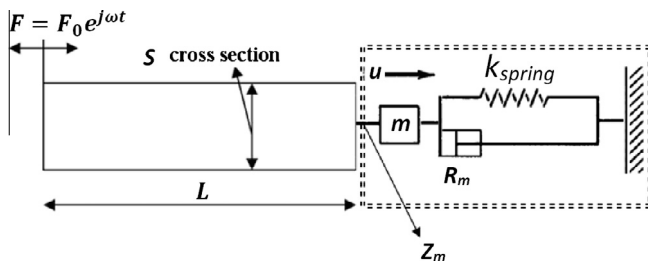


Fig. 1. Damped oscillating system at the end of an excited cylinder layer.

$$\begin{aligned} A &= -\frac{F_0 e^{jk^*L}}{2\omega s \rho c^*} \times \frac{1 + \frac{Z_m}{\rho s c^*}}{\frac{Z_m}{j\rho s c^*} \cos k^*L + \sin k^*L} = A_1 + jA_2 \\ B &= -\frac{F_0 e^{-jk^*L}}{2\omega s \rho c^*} \times \frac{1 - \frac{Z_m}{\rho s c^*}}{\frac{Z_m}{j\rho s c^*} \cos k^*L + \sin k^*L} = B_1 + jB_2 \end{aligned} \quad (4)$$

Particle velocity of wave is the time derivative of displacement ( $u$ )

$$\dot{u}(x, t) = \frac{F_0}{s \rho c^*} \frac{\cos[k^*(L-x)] + j\left(\frac{Z_m}{\rho s c^*}\right) \sin[k^*(L-x)]}{\left(\frac{Z_m}{\rho s c^*}\right) \cos[k^*(L-x)] + j \sin[k^*(L-x)]} e^{j\omega t} \quad (5)$$

Therefore, the input mechanical impedance of the system is given by Ref. [24] as follow:

$$Z_{int0} = \frac{F}{\dot{u}(0, t)} = s \rho c^* \frac{\left(\frac{Z_m}{\rho s c^*}\right) + j \tan k^*L}{1 + j\left(\frac{Z_m}{\rho s c^*}\right) \tan k^*L} \quad (6)$$

If it is  $Z_m = \rho s c^*$  in Eq. (6) then it is  $Z_{int0} = \rho s c^*$ . It means that behaviour of the system is completely the same as the force vibration for an infinitive layer which is excited at one end. Indeed, the expressed equations can be used for the system shown in Fig. 2.

Now, the multilayers transmission situation is shown in Fig. 3. The multilayers are excited by an actuator like PZT at left end.

The following assumptions are subsequently considered:

- The reflected wave in medium  $n$  is assumed to be non-existent because this layer is assumed to have infinite length. Then, the  $n$ th medium has an infinite length, i.e.,  $l_n = \infty$ .
- Although the bounded media may produce multiple reflections and transmissions in each layer, it is sufficient to assume that only one wave is present in each propagating direction; provides that the boundary conditions are satisfied. These waves will include all individual components;
- The PZT used to generate the incident wave consumes a part of mechanical energy and converts it into electrical energy; this part of mechanical energy will be neglected. This approximation is correct only if the transducer is of an open-circuit type. The substantial mismatch in electrical impedance between the transducer and the amplifier would indicate that little energy is lost in such a manner;
- It is assumed that the wave attenuation is only due to the constant loss factor ( $\eta$ ), and this value is independent of frequency. Attenuation, and hence heating effects, will increase with frequency due to mechanisms assumed in Ref. [16]. This assumption is logical because the loss factor is calculated from the attenuation coefficient of materials at high frequency ( $\approx 3$  MHz). It is difficult to transmit signals at frequencies higher than this across significant distances in air. However, the technique should be useful over any frequency range.

Looking at Fig. 3, a plane-attenuated longitudinal sound wave propagates from left to right through a series of  $n$  cylinder layers

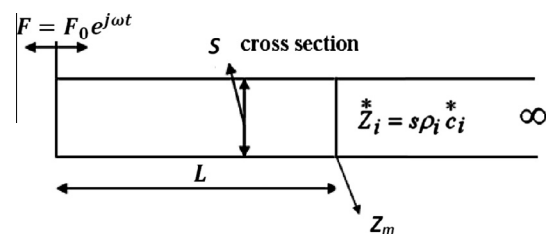


Fig. 2. Excited cylinder layer connected along an infinity length cylinder layer.

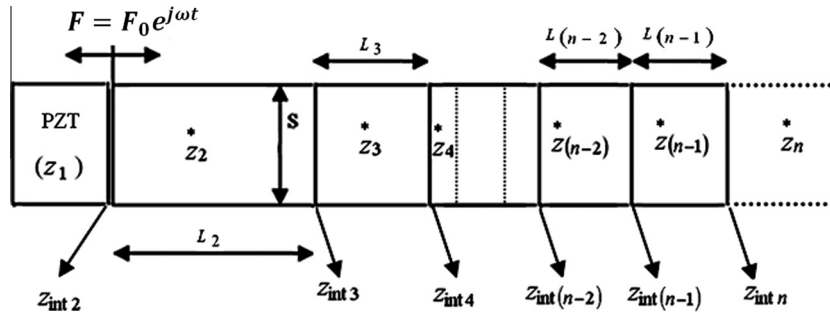


Fig. 3. Multi cylinder layer system excited at the left end by actuator.

of material with differing specific acoustic impedances. The incident wave travels through matching layer 1 ( $z_2$ ) and undergoes a series of reflections and transmissions in the subsequent layers until a transmitted wave emerges into medium  $n$ . The acoustic impedance and the length of the  $k$ th layer ( $1 \leq k \leq n$ ) are denoted as  $z_k^*$  and  $l_k$ , respectively. Therefore, the input mechanical impedance and mean power can be written for the  $i$ th layer as following (see Appendix A).

$$z_{\text{inti}} = z_i^* \times \frac{\frac{z_{\text{int}(i+1)}^*}{z_i^*} + j \tan(k_i^* l_i)}{j \left( \frac{z_{\text{int}(i+1)}^*}{z_i^*} \right) \tan k_i^* l_i + 1} \quad (7)$$

$$\langle q_i \rangle = \frac{1}{2} \omega |E_i|^* s \left( \sqrt{k_{i1}^2 + k_{i2}^2} \right) \left[ |A_i^*|^2 e^{2k_{i2}x} - |B_i^*|^2 e^{-2k_{i2}x} \right] \quad (8)$$

The physical meaning of the above equation is that the input mechanical impedance is a function of the acoustic impedance of the next matching layers, and their numbers, internal losses and thicknesses. Therefore, increasing the sound transmission energy is increased to the air by choosing favourable parameters and an optimal combination of these parameters.

## 2.2. Generation and dissipation of heat in multi-matching layers transducers with high power

There is very low (or even negligible) heat generation in transducers with low power and high frequency range. While in the airborne ultrasonic transducers with high power range (1 kW), the amount of heat produced is noticeable. The heat is generated during the sound energy transmission through the matching layers to the air and it is calculated for each matching layer based on the theory described earlier section. In practical, after determining matching layer(s) with considering attenuation, lost power and consequently amount of heat generation is calculated layer by

layer. This lost power for each matching layer is used as the heating source in ABAQUS software. The temperature distribution over the layers is determined by using ABAQUS. Fig. 4 shows a schematic of multi-matching transducer vibrating in air at room temperature.

Heat transfer between each two layers is through conduction. Additionally, heat transfer between the transducer's components and the air environment is through convection.

As shown in Fig. 4, heat transfer is from one matching layer to others and from transducer's parts to the air. Therefore, two types of heat transfer, convection and conduction are considered by assuming steady state (in equilibrium) at a certain frequency.

There is a relationship the conductive heat transfer, the amount of heat exchange between the contact layers, and the temperature between two layers.

$$H = \frac{k_{\text{heat}} A \Delta T}{L} \quad (9)$$

where  $H$  is the heat transfer through conduction (J/S),  $k_{\text{heat}}$  is heat conduction, constant transfer ( $\frac{J}{s \cdot m^2}$ ),  $\Delta T$  is temperature difference (K) between two points of a layer, and  $L$  is the distance between two points with  $\Delta T$  difference.

Another boundary condition is identical for the surface between matching layer(s) and air is the heat exchange through conduction and convection process; thus it is concluded:

$$-k_{\text{heat}} \frac{\partial T(r_o)}{\partial r} \bigg|_{r=R} = h T_{\text{air}} \quad (10)$$

The relation expressed in Eq. (10) is valid under cylindrical assumption where  $T$  is the layer's temperature and variable with radius  $r_o$  and  $r$  is distance of each point from the center,  $R$  is the radius of cylindrical shaped layer,  $T_{\text{air}}$  is air temperature around the transducer, and  $h$  is the conductive coefficient of heat transfer.

## 2.3. Genetic algorithm (GA) as solution method for the presented theory

Theoretically, the input mechanical impedance equation cannot be solved individually for more than one matching layer because the number of variables (matching layers) is greater than the number of equations. Therefore, no analytical solution exists for the calculation of the input mechanical impedance without determination of the matching layers. Furthermore, the availability of a theory that is able to find the optimal and practical acoustic impedances will increase the efficiency and the breadth of the applications of the airborne transducer. Hence, a genetic algorithm is introduced as a powerful tool to identify the optimal acoustic impedances. The detail of GA theory to determine the acoustic impedance is discussed in [25]. The genetic algorithm is applied in this work to determine the optimum matching layers to obtain

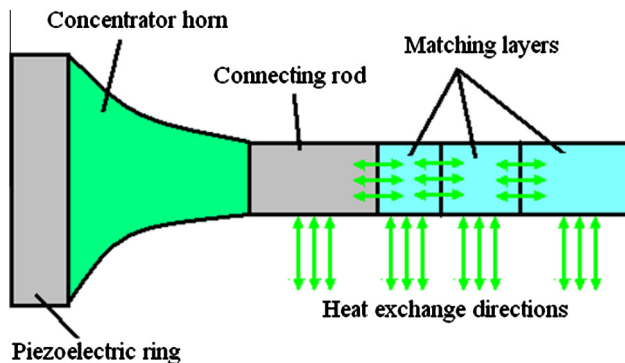


Fig. 4. Schematic of a multi-layer high power airborne transducer.

a very close input mechanical impedance of each matching layers set to the actuator source (PZT).

A code was written in an mfile in MATLAB software, which is simple and user friendly. The parameter values of the genetic algorithms used are given in Table 1, and these values were obtained after iteration.

In this program, a set of acoustic impedances that acts an initial population is generated randomly according to the number of layers. The impedance values are between that of the PZT ( $Z_p = 33 \times 10^7 \text{ kg}/(\text{m}^2 \text{ s})$ ) and air ( $Z_a = 427 \text{ kg}/(\text{m}^2 \text{ s})$ ). The fitness in this work is represented by the input mechanical impedance function; in other words, the goal is to find the best values of acoustic impedances for different numbers of matching layers to produce input mechanical impedance very close to  $33 \times 10^7 \text{ kg}/(\text{m}^2 \text{ s})$  which is correspond to the PZT. The input mechanical equation is derived by analytical methods and is used as the fitness function. For practical research, after passing the fitness function, the values of these acoustic impedances switch to the acoustic impedance of the nearest existing material from a large material database. Therefore, the acoustic impedances are ultimately chosen from the material database. Next, the input mechanical impedance is calculated with this set of acoustic impedances, and the result is compared with the stop criterion (input mechanical impedance – PZT acoustic impedance  $< 1000$ ). If the result is higher than the stop value, this chromosome is changed via a crossover operation, the calculation of the input mechanical impedance is repeated, and the result is checked again with the stop value and so on. This iteration is repeated until the input mechanical impedance becomes smaller than the stop value. The program was observed to run well for each number of layers tested experimentally, and the rich material database increases the profitability of this method. In general, the computing system used Latitude E6400, and the total CPU run time was approximately half of hour for each calculation.

### 3. Experimental setup and consideration issue

To carry out the experiments, a 1 kW ultrasonic transducer was designed and manufactured to generate the high ultrasound power required for conducting experiments. To design a transducer for plane wave propagation only, it is sufficient to model the energy source for the PZT and matching layers by adding a backing layer in the ANSYS software such that the longitudinal resonance frequency can be found by changing the backing, PZT and the matching layer(s) (especially the matching layers which are closer to the PZT side) thicknesses. This paper is part of a large research project for the design of a high-power (high-amplitude) airborne ultrasonic transmitter transducer. Therefore, 20 kHz was chosen as the working frequency in our experiments. The designed transducer consists of PZT, steel backing and aluminum matching (Fig. 5 and Table 2). These parts are placed and pressed together using screw fasteners with a torque of 170 N m. The unit must operate at the resonance condition, and therefore, an electrical matching unit is used to match the electrical circuit and ensure that the transducer always remains in the resonance condition. In this experiment, because of the ability to machine balsa wood to obtain the calculated thickness (and to achieve a  $\pm 0.01 \text{ mm}$  tolerance), this material is employed as the last matching layer



Fig. 5. Manufactured transducer according to simulation.

(air interface), and Tapox epoxy is used to couple this layer with the ultrasonic transducer. The transducer remained free of load for 36 h after addition of Tapox epoxy at the interface of the matching layer closest to the balsa. Furthermore, three same thermocouples ( $0.1^\circ \text{C}$  precision) are used to measure temperature in surface of the steel backing, aluminum and balsa matching layers. These thermocouples are installed with a constant normal force to the surface of each layer.

### 4. Results and discussion

The vibration amplitude and induced raised temperature for a number of matching layers are investigated in this study. There is a database including 297 different materials. The best matching layers are determined by GA for 1, 2 and 3 matching layers depending to the loss effect. For all cases, the assumption is that the matching layer thicknesses are calculated according to the  $(2m+1)\lambda/4$  approach previously used in the literature ( $\lambda = c/f$ , where  $\lambda$ ,  $\omega$  and  $c$  are wavelength, angular frequency and sound speed in the matching layer, respectively). Table 3 represents the specifications of the 1, 2 and 3 matching layers that are introduced by GA. For instance, polyethersulfone is the best selection from the employed database for three media or one matching layer (PZT, polyethersulfone and air). Furthermore, Table 3 shows the input power in each set of number of matching layers. Although, the potential of PZT is assumed 1 kW ( $1 \mu\text{m}$  at 20 kHz is considered as amplitude of vibration of PZT) in all cases, the capability of each set to receive and transfer this power is different and strongly depends on the selection of matching layer for receiving this power in air. However, the input power in all cases is less than nominal power of PZT due to the much lower density of the load medium (air) than vibration source (PZT). Indeed, output powers given in Table 3, are less than input power because of the internal loss in the matching layers. Hence, the differences between input and output powers show the lost power during the power transmission from PZT to the air. As shown in Table 3, the vibration amplitude of last matching layers has increased for all number of matching layers. This enhancement of the amplitude of vibration for last matching layer is at least 200 times higher than PZT ( $1 \mu\text{m}$ ). On the other hand, the temperature of matter is a direct measure of the motion of the molecules: The greater the motion is, the higher the temperature is obtained: motion requires energy: the more energy matter has the higher temperature. Rising temperature due to

Table 1  
Values of genetic algorithm parameters.

|                       |     |
|-----------------------|-----|
| Number of generations | 180 |
| Population size       | 15  |
| Number of parameters  | 2   |
| Crossover rate        | 90% |
| Mutation rate         | 10% |



**Table 2**  
Characteristic of design transducer.

| Material                      | Role                           | Diameter (mm) |                                 | Thickness (mm) | Quantity |
|-------------------------------|--------------------------------|---------------|---------------------------------|----------------|----------|
|                               |                                | Inner         | Outer                           |                |          |
| Lead zirconate titanium (PZT) | Vibration source               | 23            | 50                              | 6              | 2        |
| Al 7075-T6                    | First matching layer           | 22.6          | Smaller<br>51<br>Bigger<br>71.4 | 43             | 1        |
| Steel 304                     | Backing                        | 22.6          | 51                              | 50.6           | 1        |
| Brass                         | Connection electrode for 2 PZT | 22.8          | 51                              | 0.5            | 3        |
| Tapox epoxy                   | Second matching layer          | 72            | 72                              | 0.3            | 1        |
| Balsa wood                    | Third matching layer           | 72            | 72                              | 6.13           | 1        |
| High strength steel screw     | Mechanical connecting parts    | –             | –                               | 73.15          | 1        |

this high amplitude of vibration in high frequency is desirable to consider. Hence, the calculated lost power in each set of matching layers in MATLAB code is considered as a heat source in FEM to determine the temperature distribution in matching layers. Thus, the temperature distribution of layers is numerically calculated by ABAQUS software. Diameter of 50 mm is considered for all matching layers. The analysis of temperature distribution is time dependent, and it is performed until the time ( $t$ ) reaches to  $t = 1000$  s. The matching layers are modeled under an axi-symmetric condition. The maximum temperature is represented in Table 3 for 1000 s continues working of transducer. Figs. 6–8 show the temperature distribution for 1, 2 and 3 matching layers introduced by GA in Table 3. It is seen that maximum temperature occurs in last matching layers. In addition, the significant difference is observed between the last matching layer and other matching layers. Large vibration amplitude, high internal loss and low thermal conductivity of the last matching layer are main reasons for the temperature distribution in the matching layers. Furthermore, as shown in Table 3, the maximum determined temperatures are much higher than the allowed working temperature for the last matching layers. It is notable that all temperature values in Tables 3 and 4 are valid for 1000 s under the condition where transducer continuously works. In the condition where the transducer vibrates continuously, two procedures are implemented. The first producer is a cooling system and the second producer is used to reduce the working power in where the transducer vibrates. Table 4 lists the reliable powers for the transducer introduced in Table 3. As shown in Table 4, the maximum power of transducers without the cooling system is limited by the thermal strength restriction of the last matching layers. Mechanical strength of the last matching

layers is also important issue. Weakness mechanisms may result in failure the layers due to high amplitude of vibration.

Experimental work has been carried out to verify the approach. Table 5 represents the theoretical analysis results for the proposed transducer in powers of 0.2, 0.3 and 1 kW. It is observed in Table 5 that the maximum temperature which is generated in center of the last matching layer (Balsa wood), is higher than the flash point of Balsa (200 °C, according to the ASTM D1929) for 0.3 and 1 kW. Hence, in the first experiment, the 1 kW provided airborne ultrasonic transducer is adjusted on 20% of its nominal power (200 W). The transducer works continuously for approximately, 15 min. Fig. 9 shows temperature in three layers of the transducer. There are backing, aluminum and balsa matching layers. As shown in Fig. 9, the temperature increases rapidly to reach to the specific value after turning on the transducer and gradually increases during working. It suddenly decreases after turning it off for all transducer's elements. This phenomenon, represent that the temperature rising is affected by the friction between sensor of thermocouple and transducer's elements which are steel backing, aluminum and balsa matching layers. As illustrated in Fig. 9, the peak temperature in Balsa layer is 210 °C. Eventually the highest vibration amplitude is for balsa layer. It sounds that the high temperature can act as an indicator for determining the vibration amplitude. Therefore, the measured temperature during the working time of transducer is the temperature of the each element and the heat generation due to the friction between the sensor of thermocouple and the surface of the element of the transducer. Hence, the temperature of the each element right after turning off the transducer is measurable. The measured temperature for the parts of the transducers is compared in Table 6. The larger tem-

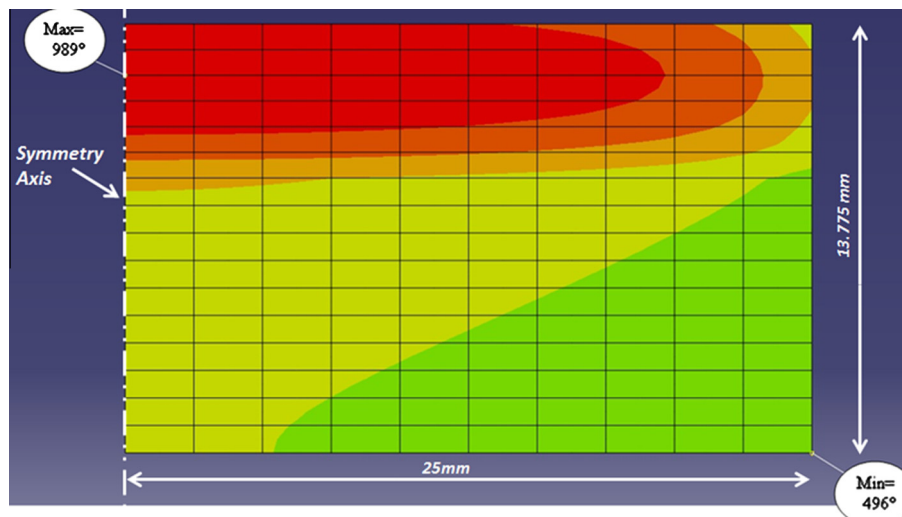


**Fig. 6.** Temperature distribution with one matching layer (poly ether sulfone).

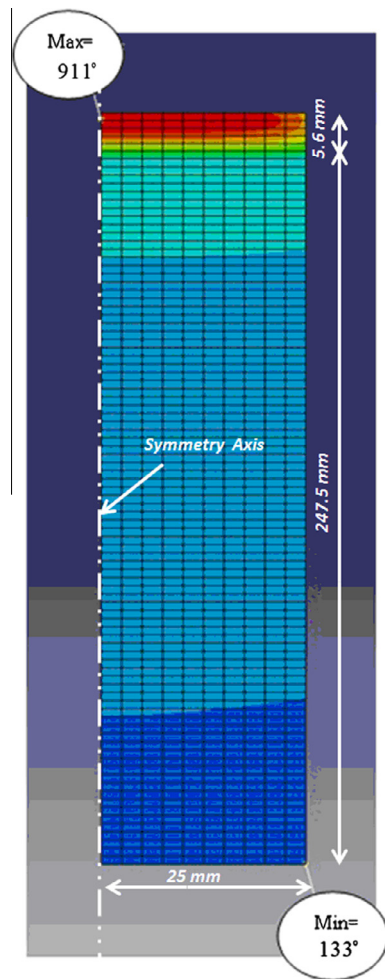


**Fig. 7.** Temperature distribution with two matching layers (polypropylene and lead alloy).

perature values are obtained with the experiments than theory because of the heat remaining in sensor. The sensor of thermocouples may slide on the surface of the transducer's element. Furthermore, additional heat is generated due to the friction of the transducer's element to each other (different material has different inertia) in experimental results. In the next step, the power of transducer is set on the 300 W. In this power, the Balsa matching layer starts to burn from the center right after 30 s of time working of the transducer. The results are shown in Fig. 10. It is interesting to note that the entire of the transducer is cool and only the balsa layer fails. This is because of the enhancement in vibration amplitude

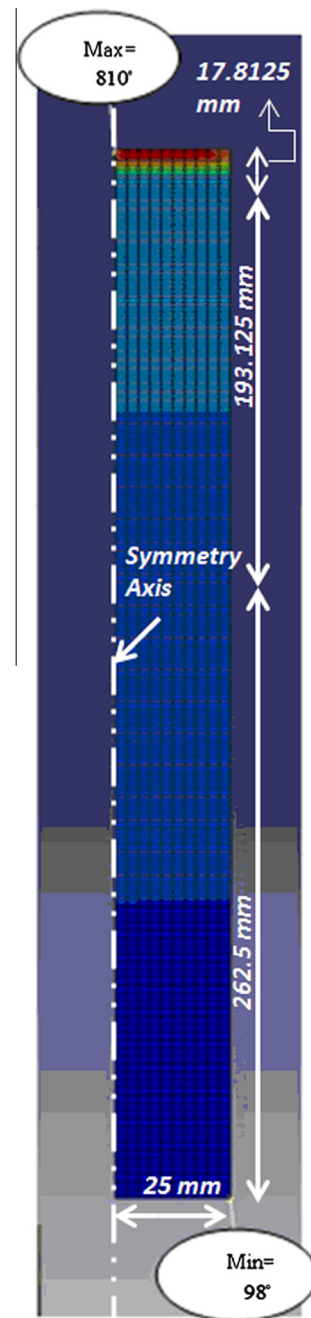


**Fig. 8.** Temperature distribution with three matching layers (copolymer acrylic, poco, and zinc).

**Table 3**  
Determined matching layers and their specification for 1, 2 and 3 matching layers.

| Matching Inyei munbei | Materials acoustic impedance (MRayl) | Input power (w) | Output power (w) | Power loss (w) | Maximum temperature (°C) within 1000 s | Working temperature (°C) | Last layer's vibration amplitude (μm) |
|-----------------------|--------------------------------------|-----------------|------------------|----------------|--|--------------------------|---------------------------------------|
| 1                     | Poly ether solphonc (0.131)          | 420             | 350              | 70             | 989                                    | 210                      | 227                                   |
| 2                     | Lead Alloy(21.5)                     | 420             | 383              | 37             | 911                                    | 160                      | 232                                   |
|                       | Titanium (23.7)                      | 320.6           | 290.2            | 30.4           | 778                                    | 210                      | 208                                   |
| 3                     | Zinc (often very granular) (29.6)    | 502             | 354              | 48             | 810                                    | 100                      | 234                                   |
|                       | Poco-DFP-1 (5–61)                    |                 |                  |                |  |                          |                                       |
|                       | Vinylc/acrylic copolymer (0.074)     |                 |                  |                |  |                          |                                       |
|                       | Ecosorb-MF 116 (9.02)                | 579.5           | 543              | 36.5           | 750                                    | 165                      | 272                                   |
|                       | Poco-DFP-1 (5.61)                    |                 |                  |                |  |                          |                                       |
|                       | Mixed cellulose esters 1 (0.094)     |                 |                  |                |  |                          |                                       |

**Table 4**

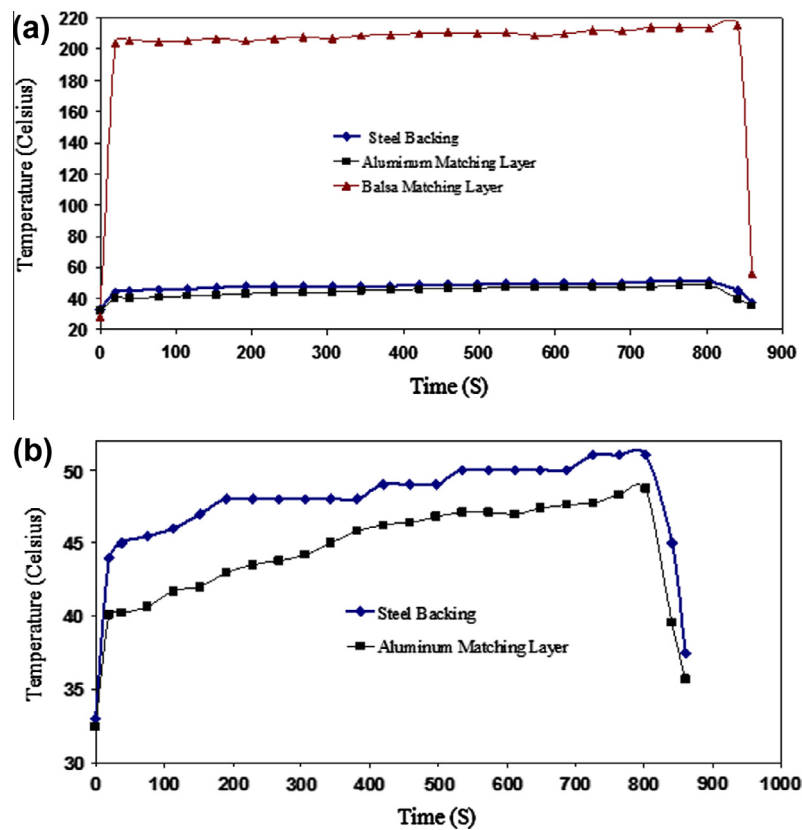
Balanced power considering thermal reliability coefficient.

| Matching layer number | Materials acoustic impedance (MRayl) |                          |                                  | Input power (W) | Output power (W) | Power loss (w) | Maximum temperature (°C) within 1000 s | PZT layer's vibration amplitude (μm) | Last layer's vibration amplitude (μm) |
|-----------------------|--------------------------------------|--------------------------|----------------------------------|-----------------|------------------|----------------|--|--------------------------------------|---------------------------------------|
| 1                     | Poly ether solphone (0.131)          |                          |                                  | 42.5            | 31.5             | 11             | 178                                    | 0.3                                  | 68.2                                  |
| 2                     | Titanium (23.7)                      | Polyethersulfone (0.131) |                                  | 105.4           | 91.8             | 13.6           | 187                                    | 0.45                                 | 120.05                                |
| 3                     | Ecosorb-MF 116 (9.02)                | Poco DFP-1 (5.61)        | Mixed cellulose esters 1 (0.091) | 184             | 176              | 8              | 155                                    | 0.48                                 | 128                                   |

**Table 5**

Information obtained from the theory to carry out the experiments.

| Material (MRay acoustic impedance) |                    |              | Power (W) |       |               | Maximum temperature | Balsa's vibration amplitude (μm) | Piezoelectric's vibration amplitude (μm) |
|------------------------------------|--------------------|--------------|-----------|-------|---------------|---------------------|----------------------------------|--|
|                                    |                    |              | Output    | Input | Piezoelectric |                     |                                  |  |
| Aluminum (17.33)                   | Tapox epoxv (2.76) | Balsa (0.08) | 156       | 348   | 1000          | 625                 | 168                              | 1  |
|                                    |                    |              | 116       | 190   | 300           | 217                 | 98                               | 0.536                                    |
|                                    |                    |              | 100       | 153   | 200           | 50.13               | 63                               | 0.438                                    |

**Fig. 9.** Temperature variation versus time (a) all layers and (b) backing and matching layers.**Table 6**

Comparison of measured temperature between theory and experiment.

|            | Steel (backing layer) | Aluminum (first matching layer) | Balsa (second matching layer) |
|------------|-----------------------|---------------------------------|-------------------------------|
| Theory     | 28.25                 | 27.1                            | 50.13                         |
| Experiment | 37.5                  | 35.7                            | 56                            |

of wooden material and consequently increasing the temperature due to the internal loss of matching layers. Therefore, it leads to burn and damage the matching layer. The results in Fig. 10 can validate the theoretical results that the temperature increase occurs

in last matching layer due to the higher amplitude of vibration. The maximum temperature happens in center of the last matching layer in high power airborne transducers. Therefore, the analysis used for low power is incomplete for the high power transducers



Fig. 10. Burned wooden matching layer at 300 W of power.

(low frequency and high amplitude). The challenge is addressed to both thermally and mechanically. The results show that the work temperature is extremely high and it occurs in the last matching layer. The layer is in contact with the air and consists typically of materials with low thermal strength and high internal loss. The induced temperature with respect to thermal loss causes burning or melting the matching layers in high power airborne ultrasonic transducers.

## 5. Conclusion

The present paper shows results from a theoretical and experimental study. It introduces and discusses the effects of the amplitude of vibration and induced temperature distribution on high power airborne ultrasonic transducers' performance. The optimum acoustic impedances of the transducer matching layers were determined by individual calculations using GA as the first step. Afterwards, it has been shown that the amplitude of vibration increases significantly for low acoustic impedance matching layers. This enhancement is maximum and approximately 200 times higher for the last matching layer where it has the similar interface with the air than the amplitude of the vibration of the source (PZT), while transferring the 1 kW is target. Furthermore, it is shown that, heat generation induced by the high amplitude of vibration is one of the most critical issues in high power airborne ultrasonic transducers. One can improve the design of mismatching layers in order to better wave transmission into the air. Theoretically, it is expressed that the temperature in last matching layer with the maximum vibration amplitude is high enough to melt or burn the matching layers. To verify the promising approach by the theory, the effect of the amplitude of vibration on the induced temperature is investigated experimentally. The results from the theory and experiments are compared and clearly experimental results are consistent with the theoretical predictions.

## Appendix A. Power equation determination

For a  $i$ th matching layer of multi matching layer system shown in Fig. 3, the displacement is expressed by:

$$\begin{aligned} u_i(x, t) &= (A_{i1} + jA_{i2})e^{j(\omega t - (k_{i1} + jk_{i2})x)} + (B_{i1} + jB_{i2})e^{j(\omega t + (k_{i1} + jk_{i2})x)} \\ &= (A_{i1} + jA_{i2})e^{k_{i2}x}e^{j(\omega t - k_{i1}x)} + (B_{i1} + jB_{i2})e^{-k_{i2}x}e^{j(\omega t + k_{i1}x)} \\ &= A_{i1}e^{k_{i2}x}\cos(\omega t - k_{i1}x) - A_{i2}e^{k_{i2}x}\sin(\omega t - k_{i1}x) \\ &\quad + B_{i1}e^{-k_{i2}x}\cos(\omega t + k_{i1}x) - B_{i2}e^{-k_{i2}x}\sin(\omega t + k_{i1}x) \\ &\quad + j[A_{i1}e^{k_{i2}x}\sin(\omega t - k_{i1}x) + A_{i2}e^{k_{i2}x}\cos(\omega t - k_{i1}x) \\ &\quad + B_{i1}e^{-k_{i2}x}\sin(\omega t + k_{i1}x) + B_{i2}e^{-k_{i2}x}\cos(\omega t + k_{i1}x)] \quad (A1) \end{aligned}$$

By using time and location derivative of displacement equation, particle velocity and force of the wave is obtained by the following equations:

$$\dot{u}_i(x, t) = j\omega u_i(x, t) \quad (A2)$$

$$\begin{aligned} F_i &= -sE_i^* \frac{\partial u_i}{\partial x} \\ &= -s(\text{real}E_i^* + j\text{mag}E_i^*)[-A_{i1} - jA_{i2}]e^{k_{i2}x}e^{j(\omega t - k_{i1}x)} + (B_{i1} \\ &\quad + jB_{i2})e^{-k_{i2}x}e^{j(\omega t + k_{i1}x)}] \quad (A3) \end{aligned}$$

$$\begin{aligned} F_i &= -sE_i^* \frac{\partial u_i}{\partial x} \\ &= -s(\text{real}E_i^* + j\text{mag}E_i^*)[-A_{i1}e^{k_{i2}x}\cos(\omega t - k_{i1}x) + A_{i2}e^{k_{i2}x} \\ &\quad \times \sin(\omega t - k_{i1}x) + B_{i1}e^{-k_{i2}x}\cos(\omega t + k_{i1}x) - B_{i2}e^{-k_{i2}x} \\ &\quad \times \sin(\omega t + k_{i1}x) + j[-A_{i1}e^{k_{i2}x}\sin(\omega t - k_{i1}x) - A_{i2}e^{k_{i2}x} \\ &\quad \times \cos(\omega t - k_{i1}x) + B_{i1}e^{-k_{i2}x}\sin(\omega t + k_{i1}x) + B_{i2}e^{-k_{i2}x} \\ &\quad \times \cos(\omega t + k_{i1}x)]] \quad (A4) \end{aligned}$$

Instantaneous power is defined as:

$$q_i = F_i \cdot \dot{u}_i = -E_i^* s \frac{\partial u_i(x, t)}{\partial x} \cdot \frac{\partial u_i(x, t)}{\partial t} \quad (A5)$$

By inserting Eqs. (A1), (A2), (A3), (A4) into (A5), the instantaneous can be written as:

$$\begin{aligned} q_i &= f_i \cdot \dot{u}_i \\ &= -s_i(\text{real}E_i^* + j\text{mag}E_i^*)[-A_{i1}e^{k_{i2}x}\cos(\omega t - k_{i1}x) + A_{i2}e^{k_{i2}x} \\ &\quad \times \sin(\omega t - k_{i1}x) + B_{i1}e^{-k_{i2}x}\cos(\omega t + k_{i1}x) - B_{i2}e^{-k_{i2}x} \\ &\quad \times \sin(\omega t + k_{i1}x) + j[-A_{i1}e^{k_{i2}x}\sin(\omega t - k_{i1}x) - A_{i2}e^{k_{i2}x} \\ &\quad \times \cos(\omega t - k_{i1}x) + B_{i1}e^{-k_{i2}x}\sin(\omega t + k_{i1}x) + B_{i2}e^{-k_{i2}x} \\ &\quad \times \cos(\omega t + k_{i1}x)]] \times j\omega[(A_{i1} + jA_{i2})e^{j(\omega t - (k_{i1} + jk_{i2})x)} + (B_{i1} \\ &\quad + jB_{i2})e^{j(\omega t + (k_{i1} + jk_{i2})x)}] \\ &= (A_{i1} + jA_{i2})e^{k_{i2}x}e^{j(\omega t - k_{i1}x)} + (B_{i1} + jB_{i2})e^{-k_{i2}x}e^{j(\omega t + k_{i1}x)} \\ &= A_{i1}e^{k_{i2}x}\cos(\omega t - k_{i1}x) - A_{i2}e^{k_{i2}x}\sin(\omega t - k_{i1}x) + B_{i1}e^{-k_{i2}x} \\ &\quad \times \cos(\omega t + k_{i1}x) - B_{i2}e^{-k_{i2}x}\sin(\omega t + k_{i1}x) + j[A_{i1}e^{k_{i2}x} \\ &\quad \times \sin(\omega t - k_{i1}x) + A_{i2}e^{k_{i2}x}\cos(\omega t - k_{i1}x) + B_{i1}e^{-k_{i2}x} \\ &\quad \times \sin(\omega t + k_{i1}x) + B_{i2}e^{-k_{i2}x}\cos(\omega t + k_{i1}x)] \quad (A6) \end{aligned}$$

Finally by employing some mathematical work, the mean power can be written as:

$$\langle q_i \rangle = \frac{1}{2}\omega|E_i|^*s\left(\sqrt{k_{i1}^2 + k_{i2}^2}\right)\left[|A_i^*|^2e^{2k_{i2}x} - |B_i^*|^2e^{-2k_{i2}x}\right] \quad (A7)$$

where the coefficients are defined as:



$$\begin{aligned}
A_i &= -\frac{F_{\text{inti}} e^{jk_i^* l_i}}{2\omega z_i^* s} \times \frac{1 + \frac{z_{\text{int}(i+1)}^*}{z_i^*}}{\frac{z_{\text{int}(i+1)}^*}{jz_i^*} \cos k_i^* l_i + \sin k_i^* l_i} \\
&= \frac{z_{\text{inti}} V_i(0, t) e^{jk_i^* l_i}}{2\omega z_i^*} \times \frac{1 + \frac{z_{\text{int}(i+1)}^*}{z_i^*}}{\frac{z_{\text{int}(i+1)}^*}{jz_i^*} \cos k_i^* l_i + \sin k_i^* l_i} \\
&= \frac{z_{\text{inti}} V_i(0, t) e^{-k_2 l_i} \times e^{jk_1 l_i}}{2\omega z_i^*} \times \frac{1 + \frac{z_{\text{int}(i+1)}^*}{z_i^*}}{\frac{z_{\text{int}(i+1)}^*}{jz_i^*} \cos k_i^* l_i + \sin k_i^* l_i} \quad (A8)
\end{aligned}$$

$$\begin{aligned}
B_i &= -\frac{F_{\text{inti}} e^{-jk_i^* l_i}}{2\omega z_i^*} \times \frac{1 - \frac{z_{\text{int}(i+1)}^*}{z_i^*}}{\frac{z_{\text{int}(i+1)}^*}{jz_i^*} \cos k_i^* l_i + \sin k_i^* l_i} \\
&= \frac{z_{\text{inti}} V_i(0, t) e^{-jk_i^* l_i}}{2\omega z_i^*} \times \frac{1 - \frac{z_{\text{int}(i+1)}^*}{z_i^*}}{\frac{z_{\text{int}(i+1)}^*}{jz_i^*} \cos k_i^* l_i + \sin k_i^* l_i} \\
&= \frac{z_{\text{inti}} V_i(0, t) e^{k_2 l_i} \times e^{-jk_1 l_i}}{2\omega z_i^*} \times \frac{1 - \frac{z_{\text{int}(i+1)}^*}{z_i^*}}{\frac{z_{\text{int}(i+1)}^*}{jz_i^*} \cos k_i^* l_i + \sin k_i^* l_i} \quad (A9)
\end{aligned}$$

$$F_{\text{inti}} = Z_{\text{inti}} \times V_i \quad (A10)$$

$$Z_{\text{inti}} = Z_i * \frac{\frac{z_{\text{int}(i+1)}^*}{z_i^*} + j \tan(k_i * l_i)}{j(\frac{z_{\text{int}(i+1)}^*}{z_i^*}) \tan k_i * l_i + 1} \quad (A11)$$

## References

- [1] C.S. Desilets, J.D. Fraser, G.S. Kino, The design of efficient broadband piezoelectric transducers, *IEEE Transactions Sonics Ultrasonics* SU-23 (3) (1978) 115–125.
- [2] P.J. Highmore, Impedance matching at ultrasonic frequencies using thin transition layers, in: *Ultrasonics International Conference Proceedings*, London, 1973, p. 112.
- [3] L.C. Lynnworth, Ultrasonic impedance matching from solids to gases, *IEEE Transactions Sonics Ultrasonics* SU-12 (2) (1965) 37–48.
- [4] M. Tone, T. Yano, A. Fukumoto, High frequency ultrasonic transducer operating in air, *Japanese Journal of Applied Physics* 23 (1984) 436–438.
- [5] T. Gudra, K.J. Opielinski, Influence of acoustic impedance of multilayer acoustic systems on the transfer function of ultrasonic airborne transducers, *Ultrasonics* 40 (2002) 457–463.
- [6] K.J. Opielinski, T. Gudra, Influence of the thickness of multilayer matching systems on the transfer function of ultrasonic airborne transducer, *Ultrasonics* 40 (2002) 465–469.
- [7] T. Gudra, K.J. Opielinski, Ultrasonic transducers working in the air with the continuous wave within the 50–500 kHz frequency range, *Ultrasonics* 42 (2004) 453–458.
- [8] G. Kossor, The effects of backing and matching on the performance of piezoelectric ceramic transducers, *IEEE Transactions Sonics Ultrasonics* SU-13 (1) (1966) 20–30.
- [9] M.I. Haller, B.T. Khuri-Yakub, Composites for ultrasonic air transducers, *IEEE Ultrasonics Symposium* (1992) 937–939.
- [10] M. Toda, Narrowband impedance matching layer for high efficiency thickness mode ultrasonic transducers, *IEEE Transactions on Ultrasonics, Ferroelectrics, and Frequency Control* 49 (2002) 299–306.
- [11] M. Toda, New type of matching layer for air-coupled ultrasonic transducers, *IEEE Transactions on Ultrasonics, Ferroelectrics, and Frequency Control* 49 (2002) 972–979.
- [12] S.P. Kelly, G. Hayward, T.E.G. Alvarez-Arenas, Characterisation and assessment of an integrated matching layer for air coupled ultrasonic applications, *IEEE Transactions on Ultrasonics, Ferroelectrics and Frequency Control* 51 (10) (2004) 1314–1323.
- [13] T.E. Gomez, A. Arenas, F.R. Montero de Espinosa, M. Moner-Girona, E. Rodríguez, A. Roig, E. Molins, Viscoelasticity of silica aerogels at ultrasonic frequencies, *Applied Physics* 81 (2002) 1198–1200.
- [14] E. Tomás, Álvarez-Arenas Gómez, R. Francisco, Montero de Espinosa, piezoelectric transducers for air-coupled operation in the frequency range 0.3–2.5 MHz, *Ultrasonics* (2002).
- [15] S.N. Ramadas, R.L. O'Leary, A. Gachagan, Ultrasonic sensor design for NDE application: design challenges & considerations, in: *Proceedings of the National Seminar & Exhibition on Non-Destructive Evaluation*, Glasgow, 2009.
- [16] T.E. Gomez, A. Arenas, Acoustic impedance matching of piezoelectric transducers to the air, *IEEE Transactions on Ultrasonics, Ferroelectrics, and Frequency Control* 51 (2004) 624–634.
- [17] T.H. Gan et al., The use of broad band acoustic transducers and pulse-compression techniques for air-coupled ultrasonic imaging, *Ultrasonics* 39 (2001) 181–194.
- [18] T.H. Gan et al., Preliminary studies of a novel air-coupled ultrasonic inspection system for food containers, *Journal of Food Engineering* 53 (2002) p315–323.
- [19] A. David, Hutchins, et al., Through-transmission imaging of solids in air using ultrasonic gas-jet waveguides, *IEEE Transactions on Ultrasonics, Ferroelectrics, and Frequency Control* 50 (2003) 1509–1515.
- [20] A. David, Hutchins, et al., High-resolution, air-coupled ultrasonic imaging of thin materials, *IEEE transactions on Ultrasonics, Ferroelectrics, and Frequency Control* 50 (2003) 1516–1525.
- [21] A. David, Hutchins, et al., A swept frequency multiplication technique for air-coupled ultrasonic NDE, *IEEE Transactions on Ultrasonics, Ferroelectrics, and Frequency Control* 51 (2004) 1271–1280.
- [22] P. Pallav et al., Air-coupled ultrasonic evaluation of food materials, *Ultrasonics* 49 (2009) 244–253.
- [23] W. Ke et al., 3D finite element simulations of an air-coupled ultrasonic NDT system, *NDT&E International* 42 (2009) 524–533.
- [24] L.E. Kinsler, *Fundamentals of Acoustics*, fourth ed., John Wiley & Sons Inc., 2000.
- [25] S. Saffar, A. Abdullah, Determination of acoustic impedances of multi matching layers for narrowband ultrasonic airborne transducers at frequencies <2.5 MHz – application of a genetic algorithm, *Journal of Ultrasonics* 52 (2012) 169–185.